ACS APPLIED MATERIALS & INTERFACES

Research Article

www.acsami.org

# Synthesis-Microstructure-Performance Relationship of Layered Transition Metal Oxides as Cathode for Rechargeable Sodium Batteries Prepared by High-Temperature Calcination

Man Xie,[†,‡,#] Rui Luo,[†,#] Jun Lu,[§,#] Renjie Chen,*[,†,‡] Feng Wu,[†,‡] Xiaoming Wang,[†] Chun Zhan,[§] Huiming Wu,[§] Hassan M. Albishri,[∥] Abdullah S. Al-Bogami,[∥] Deia Abd El-Hady,[∥] and Khalil Amine*[,§,∥]

[†]Beijing Key Laboratory of Environmental Science and Engineering, School of Chemical Engineering and Environment, Beijing Institute of Technology, Beijing, 100081, China

[‡]National Development Center of High Technology Green Materials, Beijing, 100081, China

[§]Chemical Sciences and Engineering Division, Argonne National Laboratory, 9700 South Cass Avenue, Lemont, Illinois 60439, United States

[∥]King Abdulaziz University, Faculty of Science, Jeddah, 80203, Saudi Arabia

**ABSTRACT:** Research on sodium batteries has made a comeback because of concern regarding the limited resources and cost of lithium for Li-ion batteries. From the standpoint of electrochemistry and economics, Mn- or Fe-based layered transition metal oxides should be the most suitable cathode candidates for affordable sodium batteries. Herein, this paper reports a novel cathode material, layered $Na_{1+x}(Fe_{y/2}Ni_{y/2}Mn_{1-y})_{1-x}O_2$ ($x$ = 0.1−0.5), synthesized through a facile coprecipitation process combined with subsequent calcination. For such cathode material calcined at 800 °C for 20 h, the Na/$Na_{1+x}(Fe_{y/2}Ni_{y/2}Mn_{1-y})_{1-x}O_2$ ($x$ = 0.4) electrode exhibited a good capacity of 99.1 mAh $g^{-1}$ (cycled at 1.5−4.0 V) and capacity retention over 87% after 50 cycles. Optimization of this material would make layered transition metal oxides a strong candidate for the Na-ion battery cathode.

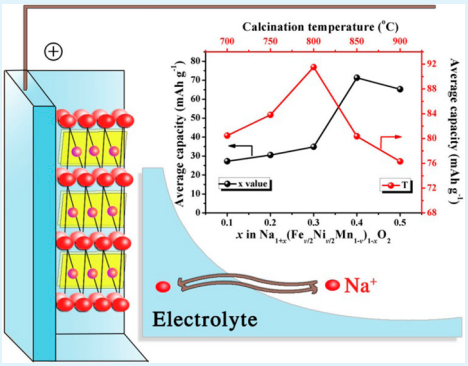


**KEYWORDS:** *Na-ion batteries, cathode, layered structure, transition-metal oxide, calcination*

## 1. INTRODUCTION

There has been a resurgence of research in Na-ion battery chemistry in recent years because of its abundant reserves and potential cost advantages.[1−5] To date, inspired by the similar intercalation chemistry for Na- and Li-ion batteries, researchers have explored many compounds as candidate cathodes for sodium-ion batteries.[6] Among these candidates, layered $NaMO_2$ (M = Ni, Mn, Cr, Co, V, etc.) compounds are promising due to the similar attractive features to Li-ion batteries, that is, material cost, wide distribution of transition metals, high capacity, and valence state.[7−11] Although both secondary battery systems share these common characteristics, the Na-ion battery exhibits different electrochemical performance. The main difference is that the ionic radius of $Na^+$ (0.98 Å) is greater than that of $Li^+$ (0.68 Å), resulting in a tendency for Na compounds to form in a layered structure.[12] Moreover, unlike their Li analogues, most $NaMO_2$ compounds present complicated voltage profiles due to the corresponding phase transformation upon cycling.[11]

Types of insertion compounds studied for the Na-ion battery system include P2-$Na_xCoO_2$,[8,13,14] O3-$NaNiO_2$,[15] O′3-$NaVO_2$,[16] and $Na_xMnO_2$.[17,18] In addition, O3-type $\alpha$-$NaFeO_2$[19] is surprisingly electrochemically active (90 mAh $g^{-1}$). Recently, Ti-based materials (Na (M, $Ti^{4+}$)$O_2$, where M = Ni, Co, etc.) have been tested as cathodes for sodium-ion batteries.[20] Sodium transition metal oxides with appropriate stoichiometry are capable of reversible Na intercalation but with limited capacity and rate performance.[12] Several strategies have been employed to overcome these problems. For example, solid solutions of $Na_xMO_2$ phases such as O3-type $Na_{1-x}Ni_{0.5}Mn_{0.5}O_2$[21] and O3-$Na_xMn_{1-y}Fe_yO_2$[22] are known to exhibit better electrochemical performance. Yabuuchi et al.[23] reported the electrochemical performance of layered Na insertion hosts of P2- and O3-$Na_x[Fe_{1/2}Mn_{1/2}]O_2$ and found that O3-type delivered 100−110 mAh $g^{-1}$ in the voltage range of 1.5−4.2 V at C/20, while P2-type delivered a higher capacity of 190 mAh $g^{-1}$ at the same condition. In addition, in a study of the electrochemical properties of $Na[Ni_{1/3}Fe_{1/3}Mn_{1/3}]O_2$,[24] the $R\bar{3}m$ layered structure was stable after extensive cycling, as revealed by the X-ray diffraction (XRD) pattern of the cathode material after 123 cycles. On the basis of the experimental evidence, Li-substituted $Na_{1.0}Li_{0.2}Ni_{0.25}Mn_{0.75}O_\delta$[25] oxide has been reported to have reversible Na intercalation and display smoothed charge−discharge profiles. This Li-incorporated

**Received:** July 25, 2014
**Accepted:** September 5, 2014
**Published:** September 5, 2014

  

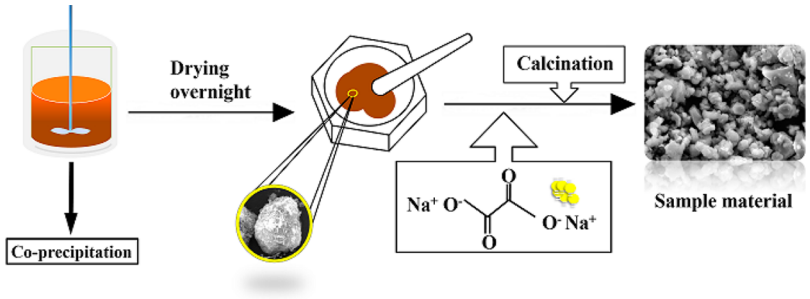


**Figure 1.** Schematic illustration of the synthetic route used to prepare cathode materials.

cathode material delivered 95−100 mAh $g^{-1}$ in the voltage range of 2.0−4.2 V and exhibited good battery performance. It should be noted that this compound can be regarded as in the family of "alkali-excess" materials such as $Li_{1.2}Ni_{0.2}Mn_{0.6}O_2$.[26,27]

Because of the elemental abundance and high capacity, the Ni-incorporated $Na_xMn_{1-y}Ni_yO_2$ is considered to be one of the most attractive cathode materials for the sodium battery. A small amount of added Ni could decrease the content of Mn(III) in order to alleviate the Jahn−Teller distortion of Mn and stabilize the phase structure. Herein, we discuss the relationship between calcination temperature and the electrochemical properties of $Na_{1+x}(Fe_{y/2}Ni_{y/2}Mn_{1-y})_{1-x}O_2$ as an O3-type electrode in Na-ion cells. Because the detailed structure of the $Na_{1+x}(Fe_{y/2}Ni_{y/2}Mn_{1-y})_{1-x}O_2$ material has not been described previously, we do so here to provide a starting point for investigating the evolution of the structure and electrochemical performance of this alkali-excess material in the sodium-ion battery.

## 2. EXPERIMENTAL SECTION

**2.1. Materials Synthesis.** The sodium cathode compounds were synthesized using a coprecipitation-calcination process (Figure 1) that was reported earlier.[11,24,28] Coprecipitated $M(OH)_2$ precursors were synthesized by titrating stoichiometric amounts of $Fe(NO_3)_3{\cdot}9H_2O$ (99%, AR), $Ni(NO_3)_2{\cdot}4H_2O$ (98%, AR), and $MnCl_2{\cdot}4H_2O$ (99%, AR) into a NaOH (96%, AR) solution. Then, the precursors were filtered, washed three times with ionized water, and dried at 100 °C for 12 h. The dried $M(OH)_2$ precursors were ground with a stoichiometric amount of $Na_2C_2O_4$, and the powder mixture was pressed into pellets. The calcination was performed in a muffle furnace under a wide range of thermal conditions: 700−900 °C with holding times of 12−24 h.[28] The as-prepared cathode powders were stable in air, and the coprecipitation process was a facile synthesis route.

**2.2. Characterization and Electrochemical Measurements.** The morphologies of the as-prepared materials were examined by scanning electron microscopy (SEM) and energy dispersive X-ray spectroscopy (EDX). X-ray diffraction (XRD) was performed with a diffractometer (Rigaku Ultima IV) using Cu K$\alpha$ radiation. Raman spectra were obtained on a Raman spectrometer (JY Labram HR 800). Electrochemical measurement was carried out using coin-type cells. The cathodes were prepared by pasting a mixture of 80 wt % active materials, 10 wt % acetylene black, and 10 wt % polyvinylidene fluoride (PVDF) onto an aluminum foil current collector. The thickness of the cathode electrodes was controlled at 200 $\mu$m. Sodium metal was used as the counter electrode. The electrolyte consisted of 1 M $NaClO_4$ dissolved in ethyl carbonate (EC) and dimethyl carbonate (DMC) (1:1 by volume). The cells were assembled in an argon-filled glovebox and then aged for 24 h before electrochemical testing. Cyclic voltammetry (CV) and electrochemical impedance spectroscopy (EIS) measurements were performed using an electrochemical workstation (Chi 604D). Galvanostatic charge−discharge experiments were carried out between 1.5 and 4.0 V using a battery tester (Land CT2001A).

## 3. RESULTS AND DISCUSSION

**3.1. Morphology and Composition of As-Prepared Materials.** The SEM images of the as-prepared $Na_{1+x}(Fe_{y/2}Ni_{y/2}Mn_{1-y})_{1-x}O_2$ are shown in Figure 2. The micrographs reveal that the material particles consist of many amorphous primary grains, which exhibited agglomeration to varying degrees as a function of the $x$ values. As shown in Figure 2, the agglomerated particles become smaller with increased $x$ values. For the material with $x$ = 0.4 in Figure 2D, the as-prepared primary particles are seen to be dispersed and generally homogeneous with an obvious cliff structure at the edges and corners, indicating improved crystallization. Such uniform crystal morphology with small particle size is beneficial to providing sufficient contact between the cathode material and the electrolyte to promote electrochemical reactions. In contrast, the material with $x$ = 0.5, as shown in Figure 2E, reveals agglomeration to a small degree and a bigger particle size than the $x$ = 0.4 material. As is well-known, the particle size and surface morphological properties can greatly affect electrochemical and physical properties such as electrolyte wetting, surface resistance, and rate properties. This impact will be discussed later. Figure 2F presents the corresponding EDX elemental analysis result of the $x$ = 0.4 material, which indicates uniform elemental distribution on the material surface.

The XRD patterns of the as-prepared $Na_{1+x}(Fe_{y/2}Ni_{y/2}Mn_{1-y})_{1-x}O_2$ with different $x$ values are shown in Figure 3A. As can be seen, the patterns of samples for $x$ = 0.1, 0.2, and 0.3 followed a similar shape: sharp peaks in the vicinity of $2\theta$ = 16° but without obvious diffraction peaks, indicating a poorly crystalline structure. The samples of $x$ = 0.4 and 0.5 also have similar patterns with characteristic peaks in the vicinity of $2\theta$ = 42° and 16°. The narrow diffraction peaks indicate high crystallinity. The diffraction patterns of the $x$ = 0.4 and 0.5 materials are indexed to a rhombohedral lattice belonging to space group $R\bar{3}m$, which is iso-structural with O3-$NaCrO_2$. Lattice parameters are calculated to be $a$ = 2.974 Å and $c$ = 15.968 Å, and the crystallographic unit-cell volume is 122.3 $Å^3$. The high $c/a$ ratio of 5.369 (greater than 4.899) and well-resolved splitting of the XRD lines assigned to the pairs of Miller indices (006, 102) and (108, 110) are a very good indication of pure layered structure. This is also consistent with the observed ratio of relative intensities of the peaks due to (003) and (104) which is >1.0 for the pure samples ($x$ = 0.4, 0.5).We further investigated the crystallized state of $Na_{1+x}(Fe_{y/2}Ni_{y/2}Mn_{1-y})_{1-x}O_2$ for the composition $x$ = 0.4. Raman spectra have been widely used as a complementary tool to substantiate XRD results for layered compounds.[29] As can be deduced from Figure 3B, the $A_{1g}$ and $E_g$ active modes for the $x$ = 0.4 material originate from M−O symmetrical stretching and


dx.doi.org/10.1021/am5049114 | ACS Appl. Mater. Interfaces 2014, 6, 17176−17183

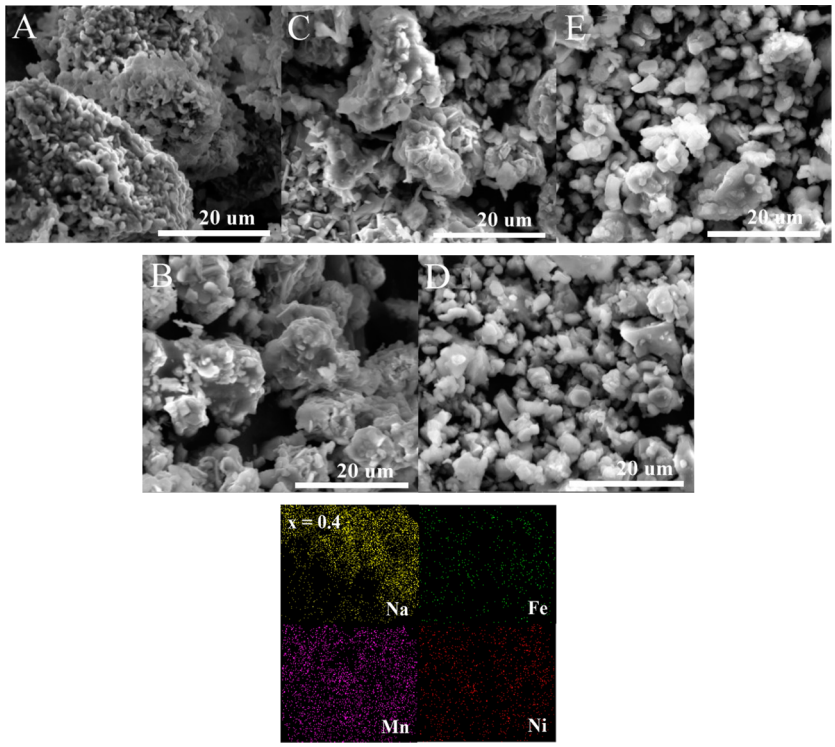


**Figure 2.** SEM images of as-prepared $Na_{1+x}(Fe_{y/2}Ni_{y/2}Mn_{1-y})_{1-x}O_2$ materials with different $x$ values: (A) 0.1, (B) 0.2, (C) 0.3, (D) 0.4, and (E) 0.5. Bottom panel: corresponding EDX elemental analysis of $x$ = 0.4. The sample magnification was selected for direct comparison.

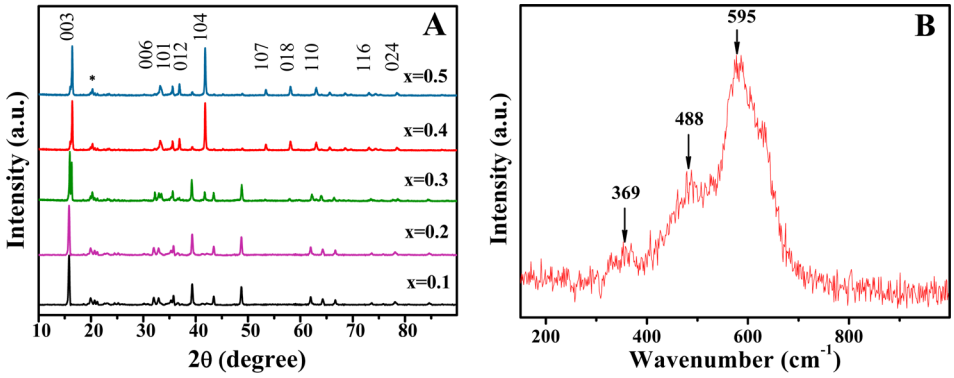


**Figure 3.** (A) XRD patterns of as-prepared $Na_{1+x}(Fe_{y/2}Ni_{y/2}Mn_{1-y})_{1-x}O_2$ electrode materials with different $x$ values and (B) Raman spectrum for the selected composition of $x$ = 0.4. All electrode materials were calcined at 850 °C for 16 h.

O−M−O bending vibrations. The Raman spectrum for the sample powder shows three obvious scattering bands at 369, 488, and 595 $cm^{-1}$ for M = Fe, Ni, and Mn, respectively. This finding shows that the sample is well crystallized.

**3.2. Electrochemical Testing of Half Cells.** The performance of the electrode materials in coin-type half-cells was characterized by galvanostatic charge−discharge cycling and CV, as shown in Figure 4. Figure 4A shows that the discharge capacities of all tested electrodes ($x$ = 0.1−0.5) gradually increase with increased $x$, and their capacity fading tendencies are different. Obviously, the $x$ = 0.4 electrode delivers the highest initial discharge capacity of 76.3 mAh $g^{-1}$, which after 50 cycles fades slightly to 70.5 mAh $g^{-1}$. The $x$ = 0.5 electrode exhibits almost as good performance. The relatively high discharge capacities and good capacity retentions of these two electrodes, compared to samples with $x$ = 0.1, 0.2, and 0.3, which contain impurities according to XRD patterns shown in Figure 3A, could be attributed to the enhanced crystallinity,[30] which is evident by clear separation of the (006)/(102) and (108)/(110) peaks (Figure 3A) and the well distributed particle morphology (Figure 2D,E). All five electrodes showed different first-cycle irreversible capacity. These differences may be attributed to the structural rearrangement of the cathode material during the first cycle, which could be related to Na-vacancy ordering or layer gliding to a new $O^{2-}$ stacking sequence and possibly a Na coordination change.[31] Another possibility is the formation of a passive film at the solid-electrolyte interface (SEI) that counts for the irreversible capacity. In contrast, Li-subsituted $Na_{1.08}Li_{0.22}Ni_{0.25}Mn_{0.75}O_\delta$ showed good reversibility and improved Coulombic efficiency during cycling.[25] We believe that the larger size of $Na^+$ compared with $Li^+$ leads to a structural rearrangement during the galvanostatically driven (de)intercalation of sodium.

To explore the reason behind this irreversible capacity loss, we obtained voltage profiles for the $x$ = 0.4 electrode on the first, second, third, and 20th cycle for a current density of 20


dx.doi.org/10.1021/am5049114 | ACS Appl. Mater. Interfaces 2014, 6, 17176−17183

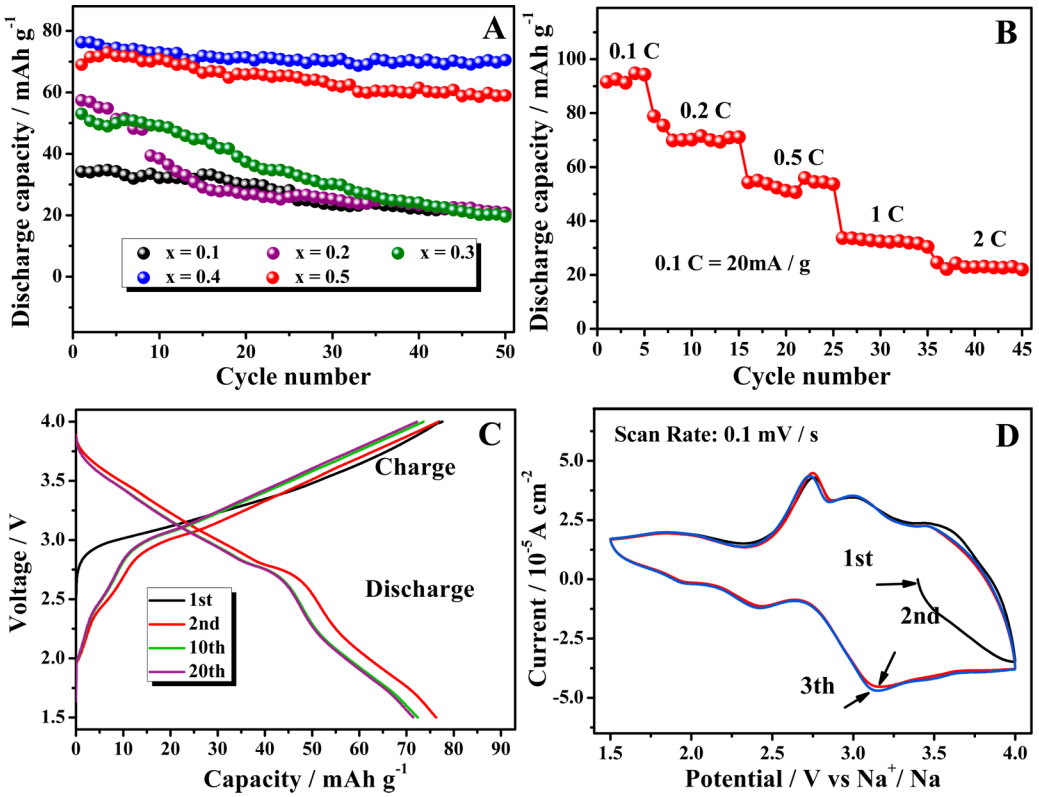


**Figure 4.** Electrochemical performance of coin-type half-cells tested in the voltage range of 1.5−4.0 V: (A) capacity versus cycle number for electrodes with $x$ = 0.1−0.5, (B) rate performance versus cycle number for $x$ = 0.4 electrode, (C) charge−discharge profiles for $x$ = 0.4 electrode at a constant current density of 20 mA $g^{-1}$ in 1st, 2nd, 10th, and 20th cycle, and (D) the 1st, 2nd, and 3rd cyclic voltammograms for $x$ = 0.4 electrode. All electrode materials were calcined at 850 °C for 16 h.

mA $g^{-1}$ (0.1 C rate) between 1.5 and 4.0 V. The voltage profiles in Figure 4C are consistent with earlier studies of layered $Na[Ni_{1/3}Fe_{1/3}Mn_{1/3}]O_2$ as the cathode, which intercalates Na within a single phase.[24] The first charge curve shows a relatively different shape compared with the others. This appearance could be ascribed to a chemical reaction in the first charge, as indicated by the CV curves shown in Figure 4D. The CV curves show three anodic peaks (3.43, 2.98, and 2.75 V) and three cathodic peaks (1.91, 2.43, and 3.17 V), which are indicative of a reversible sodium insertion-deinsertion process. For $NaNi_{1/2}Mn_{1/2}O_2$ cathode material, Zhao et al.[32] reported that the capacity originates from the $Ni^{2+}/Ni^{4+}$ redox couple and the high capacity of NMC due to the sequential oxidation sequence $Ni^{2+} \rightarrow Ni^{3+} \rightarrow Ni^{4+}$. Also, Yabuuchi et al.[23] reported on the electrochemical activity in sodium cells based on the $Fe^{3+}/Fe^{4+}$ redox in P2-$Na_x[Fe_{1/2}Mn_{1/2}]O_2$. We concluded that, within the explored potential window, the measured capacity in our cathode material originates from the $Ni^{4+}/Ni^{2+}$and $Fe^{3+}/Fe^{4+}$ redox couple.

**3.3. Effect of Calcination.** Studies on calcination after coprecipitation are rare, although the former has a significant impact on the microstructural and electrochemical properties of the cathode oxides. We selected the $x$ = 0.4 electrode to optimize the calcination conditions.

Figure 5 shows SEM images of the $x$ = 0.4 electrode material calcined at different temperatures (700−900 °C) with a holding time of 16 h. In these images, the as-prepared particles show relatively uniform particle size, surface morphology, and specific surface area at a temperature up to 800 °C. There is a distinct difference in the microstructure of the particles obtained at 900 °C, which showed severe particle agglomerates (~20−50 $\mu$m) grown from grains less than 1 $\mu$m.

Figure 6 shows the XRD patterns of the $x$ = 0.4 electrode material calcined at different temperatures for 16 h. Samples heat-treated at 700 and 750 °C do not show clear diffraction peaks, except in the vicinity of $2\theta$ = 16°, indicating a mixture with impurities during calcination, and further analysis indicates that the materials do not have a well-developed crystal structure. At higher calcination temperature, the cathode materials exhibit sharp diffraction peaks and can be indexed to a rhombohedral lattice structure with space group $R\bar{3}m$. Moreover, the higher temperature did not change the lattice structure. It should be noted that the well-developed peak at $2\theta$ = 16° strongly indicates crystalline grains at 800 °C.

Figure 7 shows the electrochemical performance of $x$ = 0.4 electrode material calcined at different temperatures for 16 h. The initial charge−discharge curves between 1.5 and 4.0 V at a current density of 20 mA $g^{-1}$ are plotted in Figure 7A. The material calcined at 700 °C delivers a relatively low initial discharge capacity of 86.3 mAh $g^{-1}$, a result of the impurity lattice structure apparent in the XRD pattern of Figure 6. The capacity increases with increasing calcination temperature up to 800 °C and reaches the highest value, 99.1 mAh $g^{-1}$, and then decreases when the temperature is over 800 °C. As can be seen from Figure 7A, all cells exhibit a sloping voltage plateau at around 3.0 V, and electrodes calcined at different temperatures exhibit similarly smoothed voltage curves. Although the origin of the plateau remains unknown, the discharge curve shapes resemble that of $Na(Ni_{1/3}Fe_{1/3}Mn_{1/3})O_2$.[25] This finding suggests that a phase transition occurred during the charge−

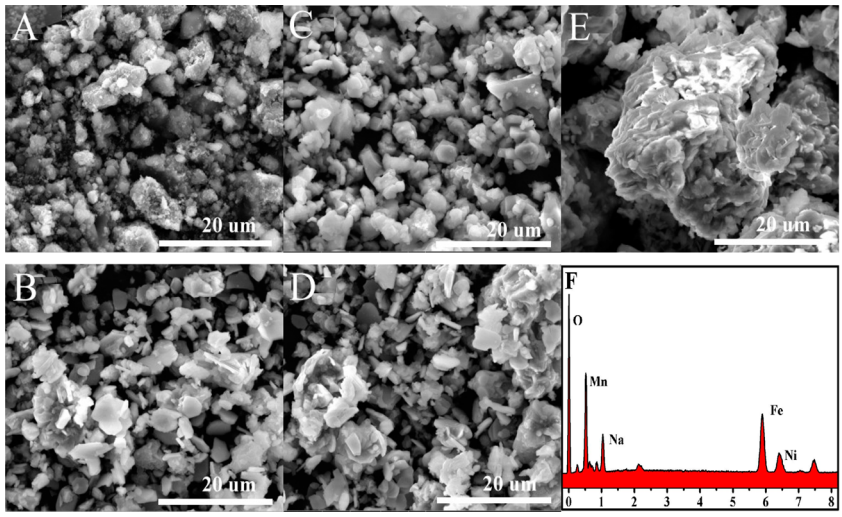


**Figure 5.** SEM images of $x$ = 0.4 electrode materials calcined at (A) 700 °C, (B) 750 °C, (C) 800 °C, (D) 850 °C, and (E) 900 °C for 16 h. (F) EDX spectra of corresponding sample calcined at 800 °C.

discharge cycles, resulting in an unknown layered-type phase in the structure due to layer gliding. This phenomenon has been observed in other Na layered oxide materials, particularly $Na_{2/3}[Ni_{1/3}Mn_{2/3}]O_2$ in Na-ion cells.[29]

Figure 7B shows the capacity over 50 cycles for the $x$ = 0.4 electrode materials calcined at different temperatures for 16 h. Although the 850 °C-calcined electrode has the highest capacity retention (shown in Figure 7B inset), it exhibits relatively low discharge capacities. The 800 °C-calcined electrode delivered the highest discharge capacity and exhibited reasonably good cycle stability.

Electrochemical impedance spectra (EIS) of the cathodes obtained at different calcination temperatures are shown in Figure 7C,D to investigate differences in the electrochemical kinetics. The EIS plots under open-circuit voltage are composed of a semicircle in the high frequency region related to the charge transfer process ($R_{ct}$) and an inclined line in the low frequency region corresponding to Warburg impedance ($Z_w$) associated with sodium-ion diffusion. The combination of $R_{ct}$ and $Z_w$ is called "faradaic impedance".[33] Note that the initial Nyquist plot at the open circuit potential consists of a semicircle and an inclined line. The initial $R_{ct}$ value for the 700 °C-calcined electrode is about 460 Ω and decreases to 230 Ω for a calcination temperature of 800 °C but increases as the calcination temperature increases. The smaller $R_{ct}$ value of the 800 °C sample suggests that the charge transfer is more facile at the electrode/electrolyte interface. This process is related to the electrochemical activation of the electrode, which facilitates sodium ion and electron transfer at the surface and penetration of liquid electrolyte into the electrode.

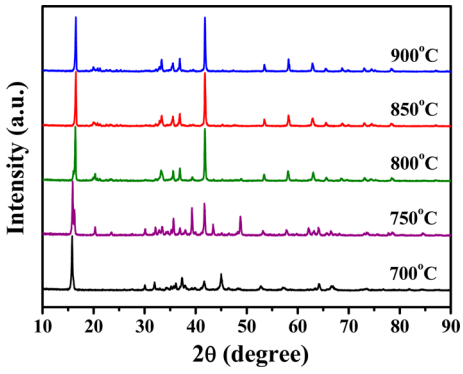


**Figure 6.** XRD patterns of $x$ = 0.4 electrode materials calcined at different temperatures with a holding time of 16 h.

We also studied the effect of calcination holding time on the structural and electrochemical properties of layered cathode materials. Figure 8 shows the SEM images of the $x$ = 0.4 electrode material calcined at 800 °C for holding times of 12–24 h. When the holding time was 12 h, the sample did not form smooth-surfaced particles, and as time increased to 20 h, the particles gradually grew into a relatively uniform particle size of ~3–8 μm and were well-distributed. The surface structure of the particles obtained for 24 h showed severe particle agglomeration of the finer primary particles less than 3 μm. Note that the longer calcination holding time introduced a deteriorated particle surface structure, suggesting an optimization time for calcination.

To further investigate the effect of calcination holding time on the crystalline structure, X-ray diffraction patterns were obtained for the $x$ = 0.4 electrode material calcined at 800 °C for holding times of 12–24 h (Figure 9). Particles obtained from 12 h holding time do not show clear diffraction peaks, except in the vicinity of $2\theta$ = 16°, indicating that the materials do not have a well-developed crystal structure. With the holding time increased to 16 h or longer, a well-developed crystalline structure formed on the basis of O3-$NaCrO_2$ with space group $R\bar{3}m$. The position of the peaks for the samples of 20 and 24 h reveal no differences. However, for the 24 h calcined sample, the peak in the vicinity of 20° decreased and split into two smaller peaks. The effect of this difference was evident in terms of the delivered capacity of the cathode materials.

Initial charge–discharge curves are shown in Figure 10A for the $x$ = 0.4 electrode material calcined at 800 °C for holding times of 12–24 h. The initial discharge capacity gradually increased with calcination time to 20 h, which showed the highest discharge capacity of 97.4 mAh $g^{-1}$ and a modest capacity fading, as evident in Figure 10B. The 24 h calcined electrode delivered a relatively low capacity. The 12 h and 16 h calcined materials showed lower initial discharge capacities but slightly rebounded in later cycles. This could be related to their

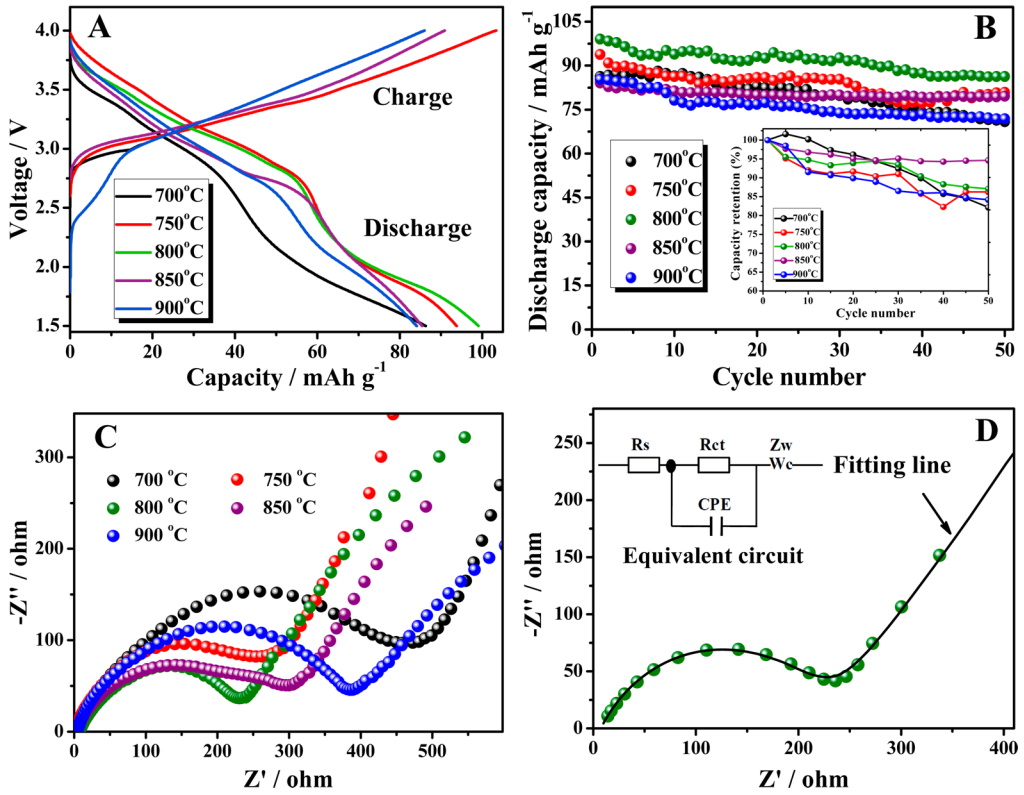


**Figure 7.** Electrochemical performance of $x$ = 0.4 electrode materials calcined at different temperatures for 16 h: (A) charge−discharge profiles, (B) capacity versus cycle number, (C) EIS at open circuit potential before charge/discharge tests, and (D) corresponding equivalent circuit and initial Nyquist plot. Half-cells cycled at a constant current density of 20 mA $g^{-1}$ between 1.5 and 4.0 V.

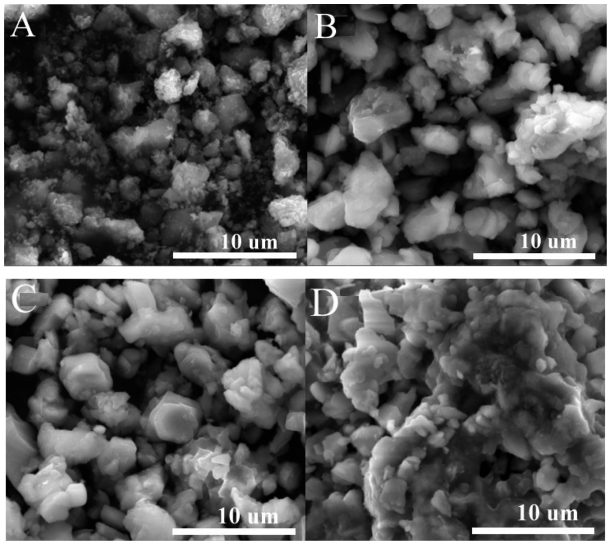


**Figure 8.** SEM images of $x$ = 0.4 electrode powders calcined at 800 °C for (A) 12 h, (B) 16 h, (C) 20 h, and (D) 24 h.

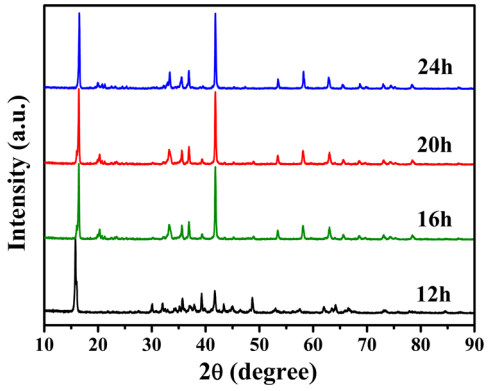


**Figure 9.** XRD patterns of $x$ = 0.4 electrode powders calcined at 800 °C for different holding times.

development of a crystalline structure, as depicted in Figure 9. Figure 10C shows the Nyquist plots of the cathodes for the different holding times. Note that the diameter of the semicircle corresponds to the charge transfer resistance at the film cathode/electrolyte interface. The diameter decreases as time increases to 20 h but increases as time reaches 24 h. The electrode calcined for 20 h exhibits a smaller $R_{total}$ than others; thus, its good electrochemical performance is probably related to its considerably smaller resistance. Figure 10D displays the variation of average capacity for 50 cycles of materials calcined for different holding times, where the material calcined for 20 h indicates the highest value. The crystallinity structure coupled with electrochemical properties shows an optimal calcination temperature (800 °C) and time (20 h) for the Na-based cathode materials.

## 4. CONCLUSION

Cathode materials of $Na_{1+x}(Fe_{y/2}Ni_{y/2}Mn_{1-y})_{1-x}O_2$ ($x$ = 0.1−0.5) were prepared by coprecipitation combined with calcination. The as-prepared material calcined at 800 °C for 20 h showed excellent specific capacity and capacity retention after 50 cycles. This alkali-excess material can serve as a benchmark for rechargeable sodium batteries and a candidate for possible low-cost energy storage applications.

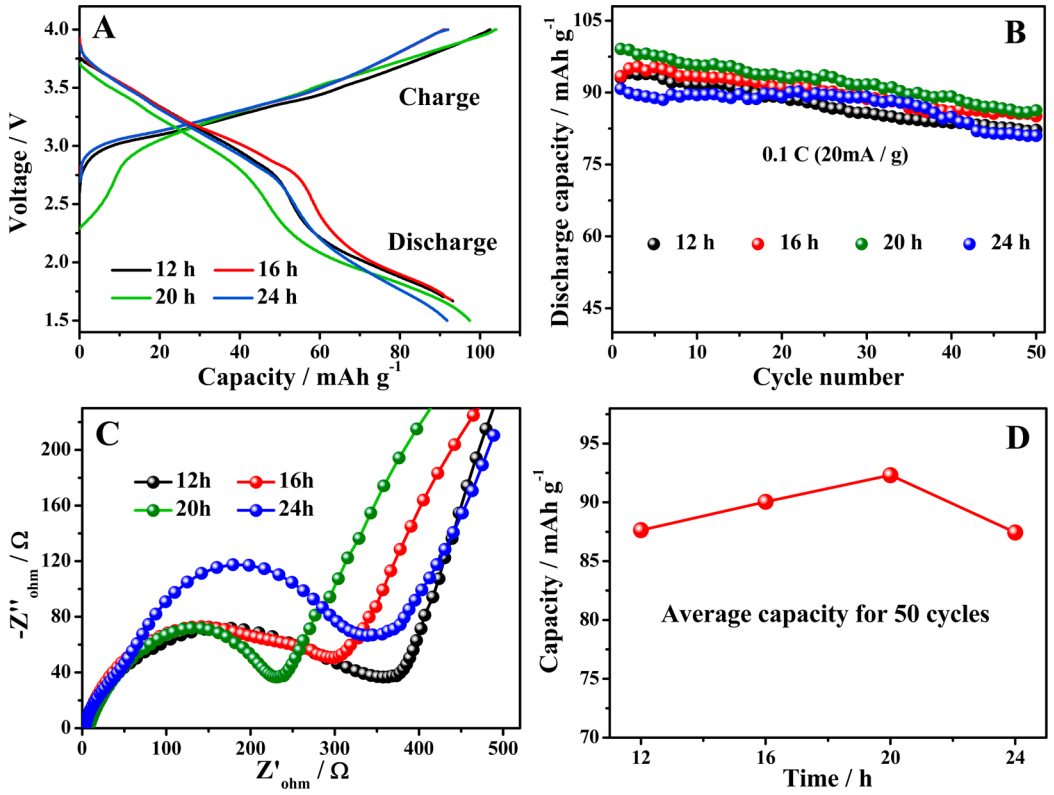


**Figure 10.** Electrochemical performance of $x = 0.4$ electrodes calcined at 800 °C for different holding times: (A) charge−discharge profiles, (B) capacity versus cycle number, (C) EIS spectra, and (D) average capacity for 50 cycles of electrodes calcined for different times. Half-cells cycled at constant current density of 20 mA $g^{-1}$ between 1.5 and 4.0 V.

## AUTHOR INFORMATION


### Corresponding Authors

*E-mail: chenrj@bit.edu.cn (R.C.).
*E-mail: amine@anl.gov (K.A.).

### Author Contributions

#M.X., R.L., and J.L. contributed equally to this work.


### Notes

The authors declare no competing financial interest.

## ACKNOWLEDGMENTS

This work was supported by the National Science Foundation of China (21373028); National 863 Program (2011AA11A256); New Century Educational Talents Plan of Chinese Education Ministry (NCET-12-0050); Beijing Novel Program (Z121103002512029); Ford University Research Program (URP) project. This work was also supported by the U.S. Department of Energy under Contract DE-AC0206CH11357 from the Vehicle Technologies Office, Department of Energy, Office of Energy Efficiency and Renewable Energy (EERE). Argonne National Laboratory, a U.S. Department of Energy Office of Science laboratory, is operated under Contract No. DE-AC02-06CH11357. This project was partially funded by the Deanship of Scientific Research (DSR), King Abdulaziz University, Jeddah under the HiCi Project (Grant No: 11-130-1434HiCi). The authors (H.M.A., D.A.E.-H., A.S.A.-B., and K.A.) thank the DSR for their technical and financial support. The authors would like to acknowledge the U.S.-China Electric Vehicle and Battery Technology Collaboration between Argonne National Laboratory and Beijing Institute of Technology.

## REFERENCES

(1) Ellis, B. L.; Makahnouk, W. R.; Makimura, Y.; Toghill, K.; Nazar, L. F. A Multifunctional 3.5V Iron-Based Phosphate Cathode for Rechargeable Batteries. *Nat. Mater.* **2007**, *6*, 749−753.

(2) Zandbergen, H.; Foo, M.; Xu, Q.; Kumar, V.; Cava, R. Sodium Ion Ordering in $Na_xCoO_2$: Electron Diffraction Study. *Phys. Rev. B* **2004**, *70*, 024101.

(3) Whitacre, J. F.; Tevar, A.; Sharma, S. $Na_4Mn_9O_{18}$ as a Positive Electrode Material for an Aqueous Electrolyte Sodium-Ion Energy Storage Device. *Electrochem. Commun.* **2010**, *12*, 463−466.

(4) Plashnitsa, L. S.; Kobayashi, E.; Noguchi, Y.; Okada, S.; Yamaki, J.-i. Performance of NASICON Symmetric Cell with Ionic Liquid Electrolyte. *J. Electrochem. Soc.* **2010**, *157*, A536−A543.

(5) Komaba, S.; Takei, C.; Nakayama, T.; Ogata, A.; Yabuuchi, N. Electrochemical Intercalation Activity of Layered $NaCrO_2$ vs. $LiCrO_2$. *Electrochem. Commun.* **2010**, *12*, 355−358.

(6) Palomares, V.; Serras, P.; Villaluenga, I.; Hueso, K. B.; Carretero-González, J.; Rojo, T. Na-Ion Batteries, Recent Advances and Present Challenges to Become Low Cost Energy Storage Systems. *Energy Environ. Sci.* **2012**, *5*, 5884−5901.

(7) Didier, C.; Guignard, M.; Denage, C.; Szajwaj, O.; Ito, S.; Saadoune, I.; Darriet, J.; Delmas, C. Electrochemical Na-Deintercalation from $NaVO_2$. *Electrochem. Solid-State Lett.* **2011**, *14*, A75−A78.

(8) Delmas, C.; Braconnier, J.-J.; Fouassier, C.; Hagenmuller, P. Electrochemical Intercalation of Sodium in $Na_xCoO_2$ Bronzes. *Solid State Ionics* **1981**, *3*−*4*, 165−169.

(9) Braconnier, J. J.; Delmas, C.; Hagenmuller, P. Etude par Desintercalation Electrochimique Des Systemes $Na_xCrO_2$ et $Na_xNiO_2$. *Mater. Res. Bull.* **1982**, *17*, 993−1000.

(10) Sauvage, F.; Laffont, L.; Tarascon, J. M.; Baudrin, E. Study of the Insertion/Deinsertion Mechanism of Sodium into $Na_{0.44}MnO_2$. *Inorg. Chem.* **2007**, *46*, 3289−3294.

(11) Xu, J.; Lee, D. H.; Clément, R. J.; Yu, X.; Leskes, M.; Pell, A. J.; Pintacuda, G.; Yang, X.-Q.; Grey, C. P.; Meng, Y. S. Identifying the

Critical Role of Li Substitution in P2−$Na_x[Li_yNi_zMn_{1-y-z}]O_2$($0 < x, y, z < 1$) Intercalation Cathode Materials for High-Energy Na-Ion Batteries. *Chem. Mater.* **2014**, *26*, 1260−1269.
(12) Sathiya, M.; Hemalatha, K.; Ramesha, K.; Tarascon, J. M.; Prakash, A. S. Synthesis, Structure, and Electrochemical Properties of the Layered Sodium Insertion Cathode Material: $NaNi_{1/3}Mn_{1/3}Co_{1/3}O_2$. *Chem. Mater.* **2012**, *24*, 1846−1853.
(13) D'Arienzo, M.; Ruffo, R.; Scotti, R.; Morazzoni, F.; Mari, C. M.; Polizzi, S. Layered $Na_{0.71}CoO_2$: A Powerful Candidate for Viable and High Performance Na-Batteries. *Phys. Chem. Chem. Phys.* **2012**, *14*, 5945−5952.
(14) Ding, J. J.; Zhou, Y. N.; Sun, Q.; Yu, X. Q.; Yang, X. Q.; Fu, Z. W. Electrochemical Properties of P2-Phase $Na_{0.74}CoO_2$ Compounds as Cathode Material For Rechargeable Sodium-Ion Batteries. *Electrochim. Acta* **2013**, *87*, 388−393.
(15) Ding, J.-J.; Zhou, Y.-N.; Sun, Q.; Fu, Z.-W. Cycle Performance Improvement of $NaCrO_2$ Cathode by Carbon Coating for Sodium Ion Batteries. *Electrochem. Commun.* **2012**, *22*, 85−88.
(16) Vassilaras, P.; Ma, X.; Li, X.; Ceder, G. Electrochemical Properties of Monoclinic $NaNiO_2$. *J. Electrochem. Soc.* **2012**, *160*, A207−A211.
(17) Didier, C.; Guignard, M.; Darriet, J.; Delmas, C. O′3-$Na_xVO_2$ System: A Superstructure for $Na_{1/2}VO_2$. *Inorg. Chem.* **2012**, *51*, 11007−11016.
(18) Doeff, M. M. Orthorhombic $Na_xMnO_2$ as a Cathode Material for Secondary Sodium and Lithium Polymer Batteries. *J. Electrochem. Soc.* **1994**, *141*, L145−L147.
(19) Ma, X.; Chen, H.; Ceder, G. Electrochemical Properties of Monoclinic $NaMnO_2$. *J. Electrochem. Soc.* **2011**, *158*, A1307−A1312.
(20) Yu, H.; Guo, S.; Zhu, Y.; Ishida, M.; Zhou, H. Novel Titanium-Based O3-Type $NaTi_{0.5}Ni_{0.5}O_2$ as a Cathode Material for Sodium Ion Batteries. *Chem. Commun.* **2014**, *50*, 457−459.
(21) Komaba, S.; Yabuuchi, N.; Nakayama, T.; Ogata, A.; Ishikawa, T.; Nakai, I. Study on the Reversible Electrode Reaction of $Na_{1-x}Ni_{0.5}Mn_{0.5}O_2$ for a Rechargeable Sodium-Ion Battery. *Inorg. Chem.* **2012**, *51*, 6211−6220.
(22) Mortemard de Boisse, B.; Carlier, D.; Guignard, M.; Delmas, C. Structural and Electrochemical Characterizations of P2 and New O3-$Na_xMn_{1-y}Fe_yO_2$ Phases Prepared by Auto-Combustion Synthesis for Na-Ion Batteries. *J. Electrochem. Soc.* **2013**, *160*, A569−A574.
(23) Yabuuchi, N.; Kajiyama, M.; Iwatate, J.; Nishikawa, H.; Hitomi, S.; Okuyama, R.; Usui, R.; Yamada, Y.; Komaba, S. P2-Type $Na_xFe_{1/2}Mn_{1/2}O_2$ Made from Earth-Abundant Elements for Rechargeable Na Batteries. *Nat. Mater.* **2012**, *11*, 512−517.
(24) Kim, D.; Lee, E.; Slater, M.; Lu, W.; Rood, S.; Johnson, C. S. Layered $Na[Ni_{1/3}Fe_{1/3}Mn_{1/3}]O_2$ Cathodes for Na-Ion Battery Application. *Electrochem. Commun.* **2012**, *18*, 66−69.
(25) Kim, D.; Kang, S.-H.; Slater, M.; Rood, S.; Vaughey, J. T.; Karan, N.; Balasubramanian, M.; Johnson, C. S. Enabling Sodium Batteries Using Lithium-Substituted Sodium Layered Transition Metal Oxide Cathodes. *Adv. Energy Mater.* **2011**, *1*, 333−336.
(26) Tabuchi, M.; Nakashima, A.; Shigemura, H.; Ado, K.; Kobayashi, H.; Sakaebe, H.; Kageyama, H.; Nakamura, T.; Kohzaki, M.; Hirano, A.; Kanno, R. Synthesis, Cation Distribution, and Electrochemical Properties of Fe-Substituted $Li_2MnO_3$ as a Novel 4V Positive Electrode Material. *J. Electrochem. Soc.* **2002**, *149*, A509−A524.
(27) Ammundsen, B.; Paulsen, J. Novel Lithium-Ion Cathode Materials Based on Layered Manganese Oxides. *Adv. Mater.* **2001**, *13*, 943−956.
(28) Chen, W.-C.; Song, Y.-F.; Wang, C.-C.; Liu, Y.; Morris, D. T.; Pianetta, P. A.; Andrews, J. C.; Wu, H.-C.; Wu, N.-L. Study on the Synthesis−Microstructure-Performance Relationship of Layered Li-Excess Nickel−Manganese Oxide as a Li-Ion Battery Cathode Prepared by High-Temperature Calcination. *J. Mater. Chem. A* **2013**, *1*, 10847−10856.
(29) Zhang, X.; Mauger, A.; Lu, Q.; Groult, H.; Perrigaud, L.; Gendron, F.; Julien, C. M. Synthesis and Characterization of $LiNi_{1/3}Mn_{1/3}Co_{1/3}O_2$ by Wet-Chemical Method. *Electrochim. Acta* **2010**, *55*, 6440−6449.
(30) Thackeray, M. M. Structural Considerations of Layered and Spinel Lithiated Oxides for Lithium Ion Batteries. *J. Electrochem. Soc.* **1995**, *142*, 2558−2563.
(31) Berthelot, R.; Carlier, D.; Delmas, C. Electrochemical Investigation of the P2-$Na_xCoO_2$ Phase Diagram. *Nat. Mater.* **2011**, *10*, 74−80.
(32) Zhao, J.; Zhao, L.; Dimov, N.; Okada, S.; Nishida, T. Electrochemical and Thermal Properties of $\alpha$-$NaFeO_2$ Cathode for Na-Ion Batteries. *J. Electrochem. Soc.* **2013**, *160*, A3077−A3081.
(33) Tan, G.; Wu, F.; Li, L.; Chen, R.; Chen, S. Coralline Glassy Lithium Phosphate-Coated $LiFePO_4$ Cathodes with Improved Power Capability for Lithium Ion Batteries. *J. Phys. Chem. C* **2013**, *117*, 6013−6021.